Large-deviation statistics of vorticity stretching in isotropic turbulence

Perry L. Johnson and Charles Meneveau

Large-deviation statistics of vorticity stretching in isotropic turbulence

Perry L. Johnson* and Charles Meneveau

Department of Mechanical Engineering and Center for Environmental
and Applied Fluid Mechanics, The Johns Hopkins University,
3400 N. Charles Street, Baltimore, Maryland 21218, USA

Abstract

A key feature of 3D fluid turbulence is the stretching/re-alignment of vorticity by the action of the strain-rate. It is shown in this paper, using the cumulant-generating function, that the cumulative vorticity stretching along a Lagrangian path in isotropic turbulence obeys a large deviation principle. As a result, the relevant statistics can be described by the vorticity stretching Cramér function. This function is computed from a Direct Numerical Simulation (DNS) dataset at a Taylor-scale Reynolds number of $Re_\lambda = 433$ and compared to those of the finite-time Lyapunov exponents (FTLE) for material deformation. As expected, the mean cumulative vorticity stretching is slightly less than that of the most-stretched material line (largest FTLE), due to the vorticity's preferential alignment with the second-largest eigenvalue of strain-rate and the material line's preferential alignment with the largest eigenvalue. However, the vorticity stretching tends to be significantly larger than the second-largest FTLE, and the Cramér functions reveal that the statistics of vorticity stretching fluctuations are more similar to those of the largest FTLE. In an attempt to relate the vorticity stretching statistics to the vorticity magnitude probability density function in statistically stationary conditions, a model Kramers-Moyal equation is constructed using the statistics encoded in the Cramér function. The model predicts a stretched-exponential tail for the vorticity magnitude PDF, with good agreement for the exponent but significant difference (35%) in the pre-factor.

---

* pjohns86@jhu.edu

I. INTRODUCTION

The production of enstrophy in three-dimensional isotropic turbulence is accomplished by the vorticity stretching mechanism, which strongly resembles the mechanism for the stretching of material lines in turbulence, though important differences can be identified. A useful concept in the study of material line stretching is the finite-time Lyapunov exponent (FTLE) of Lagrangian trajectories, which can be interpreted as the cumulative stretching of material lines along a Lagrangian path. As the statistics of FTLEs follow a large-deviation principle, it is of interest to investigate the application of large-deviation statistics to the cumulative stretching of vorticity along Lagrangian paths.

The universal or approximately universal structure of small-scale turbulence emerged from Kolmogorov's work [1] as an important theme in turbulence research. While the magnitude of velocity fluctuations is dominated by large-scale motions, the smallest scales of motion are primarily responsible for quantities representing magnitudes of velocity derivatives, such as dissipation and enstrophy [2, 3]. For this reason, a common approach to studying turbulence structure and statistics at the smallest scales is through the use of velocity gradients [4–6].

A major focus of research since Kolmorogov's 1941 hypotheses has been refinement to account for the influence of internal intermittency. Often, this has been advanced using velocity derivatives and their coarse-grained values. In 1962, Kolmogorov and Oboukov [7, 8] proposed a log-normal model (based on the Central-Limit theorem) for the spatial intermittency of coarse-grained dissipation. Parisi and Frisch [9] introduced the idea of multifractality in small-scale turbulence, essentially based on the Large-Deviation theorem rather than the Central-Limit theorem (see Frisch [10]), which was confirmed by Meneveau and Sreenivasan [11] using a measurement proxy for dissipation.

An intrinsic quality of turbulence is that it is rotational [2]. In fact, for isotropic turbulence, mean dissipation and enstrophy are directly related. Enstrophy production by the straining of existing vorticity, $\omega_i S_{ij} \omega_j$, where S_{ij} is the strain-rate tensor and ω_i is the vorticity vector, is often discussed in tandem with the idea of the cascade of energy to small scales [2] and can be related to the negative velocity derivative skewness [3] representing inter-scale transfer of energy. For this reason, the structure and statistics of enstrophy and other vorticity-related measures have also been studied extensively [12–22].

Visualization of vorticity magnitude iso-surfaces in high-resolution simulations has revealed the ubiquitous presence of tube-shaped regions of concentrated high-vorticity regions [12, 21, 23–26], confirming earlier experimental evidence [27]. Coarse-graining at various filter-widths reveals a hierarchy of vorticity tubes, smaller tubes spirally-wrapped within larger ones [28], once again suggesting the importance of multi-scale vorticity interactions in the turbulence energy cascade. The vortex tube picture has formed the basis for a number of simplified models of small-scale turbulence [29–34].

Johnson and Meneveau [35] showed that the rotation of fluid particles by vorticity strongly reduces cumulative material deformation by weakening the ability of the Cauchy-Green tensor to align with the strain-rate. This is partly responsible in reducing the deformation rate for small droplets [36] well below what the strain-rate statistics would suggest.

A key universal observation in this context is that the enstrophy production term, $\omega_i S_{ij} \omega_j$, is positive on average, meaning that enstrophy production by stretching is more prevalent than enstrophy destruction by contraction. While Taylor [37] attributed this to the stretching of material lines by invoking an equality between material deformation and vorticity stretching in inviscid flow, important differences between the two processes have been identified and investigated [19, 20, 22, 38]. These differences are manifest in the tendency of vorticity to align with the strain-rate eigenvector associated with the second-largest eigenvalue [14], while material lines tend to align slightly toward the eigenvector associated with the largest eigenvalue [39]. As a result Ref. 19 showed that vorticity stretching is on average smaller than material line stretching.

In this paper, we seek to characterize the statistics of the vorticity stretching term by looking at *cumulative* stretching along a Lagrangian path using the large deviation formalism. This characterization allows direct comparison with previous results for material deformation [35] in order to clarify similarities and differences between the two processes. Specifically, the Cramér function provides an efficient description of the asymptotic evolution of the cumulative stretching probability density function (PDF). This description enables a more detailed statistical comparison between vorticity stretching and material line stretching in turbulence. Additionally, the details of this statistical characterization can be incorporated into an approximate stochastic model for predicting features of the equilibrium distribution function of enstrophy using some existing approaches from polymer stretching studies [40, 41].

Meneveau and Sreenivasan [11] and Bershadskii et al. [42] proposed a stretched-exponential fit to the tails of the dissipation and enstrophy probability density function (PDF) based on experimental data, with exponent 0.5. With increasing computational resources in time, numerical results later confirmed that a stretched-exponential provides a good fit to the both dissipation and enstrophy PDFs, but with exponent closer to 0.25[43]. We will attempt to explain the stretched exponential behavior using statistical properties of the vorticity stretching as described by the large deviation formalism.

Background on vorticity stretching and the large-deviation formalism is given in §II. The details for the direct numerical simulation dataset and evaluation of Lagrangian statistics are given in §III. In §IV, the results of the statistical analysis are shown and discussed in terms of the Cramér function for vorticity stretching. Particular attention is paid to the relationship to material line deformation and strain-rate eigenvalue statistics. Using the Cramér function for vorticity stretching and statistical observations of diffusion, a stochastic model is constructed for the Lagrangian vorticity evolution in §V, allowing for the prediction of the vorticity magnitude PDF in stationary isotropic turbulence. Following that, §VI delineates conclusions drawn from the results in the previous sections.

II. BACKGROUND

In this section, the necessary background for this work is presented. The equations for vorticity evolution along Lagrangian paths are presented first. Following this, the large-deviation formalism is reviewed, along with its application to material deformation. Supporting arguments for the application of the large-deviation formalism to vorticity stretching are given, as well as criteria for verification.

A. Lagrangian Vorticity Evolution

In this paper, we consider forced isotropic turbulence satisfying the incompressible Navier-Stokes equations,

$$\frac{\partial u_i}{\partial t} + u_j \frac{\partial u_i}{\partial x_j} = -\frac{1}{\rho} \frac{\partial p}{\partial x_j} + \nu \frac{\partial^2 u_i}{\partial x_j \partial x_j} + f_i, \qquad \frac{\partial u_j}{\partial x_j} = 0, \tag{1}$$

where $u_i(\mathbf{x}, t)$ and $p(\mathbf{x}, t)$ are the velocity and pressure fields, respectively. The kinematic viscosity is ν and the forcing is f_i. The curl of Navier-Stokes gives an equation for the

vorticity, $\omega_i = \epsilon_{ijk}\frac{\partial u_k}{\partial x_j}$,

$$\frac{\partial \omega_i}{\partial t} + u_j \frac{\partial \omega_i}{\partial x_j} = \omega_j \frac{\partial u_i}{\partial x_j} + \nu \frac{\partial^2 \omega_i}{\partial x_j \partial x_j} + \epsilon_{ijk}\frac{\partial f_k}{\partial x_j}, \tag{2}$$

where ϵ_{ijk} is the Levi-Cevita alternating tensor.

The velocity gradient tensor can be split into symmetric and anti-symmetric components, $\frac{\partial u_i}{\partial x_j} = A_{ij} = S_{ij} + \Omega_{ij}$, with $S_{ij} = \frac{1}{2}\left(\frac{\partial u_i}{\partial x_j} + \frac{\partial u_j}{\partial x_i}\right)$ and $\Omega_{ij} = \frac{1}{2}\left(\frac{\partial u_i}{\partial x_j} - \frac{\partial u_j}{\partial x_i}\right)$. The anti-symmetric part of the velocity gradient is directly related to the vorticity by $\Omega_{ij} = -\frac{1}{2}\epsilon_{ijk}\omega_k$ and $\omega_i = -\epsilon_{ijk}\Omega_{jk}$, so that $\Omega_{ij}\omega_j = 0$. Considering low-wavenumber forcing and sufficiently high Reynolds number, the curl of the forcing can be neglected. Following Lagrangian trajectories, $x_i(t)$,

$$\frac{dx_i}{dt} = u_i(\mathbf{x}, t), \qquad x_i(t_0) = X_i, \tag{3}$$

the vorticity evolution is

$$\frac{d\omega_i}{dt} = S_{ij}\omega_j + \nu \frac{\partial^2 \omega_i}{\partial x_j \partial x_j}. \tag{4}$$

Consider the decomposition of the vorticity vector, $\omega_i = \omega\widehat{\omega}_i$, where $\omega = \sqrt{\omega_i\omega_i}$ is the vorticity magnitude and $\widehat{\omega}_i = \frac{\omega_i}{\omega}$ is the unit vector associated with the vorticity orientation. With this decomposition, the Lagrangian evolution for vorticity magnitude can be written as

$$\frac{d\omega}{dt} = \widehat{\omega}_i S_{ij}\widehat{\omega}_j \omega + \nu\widehat{\omega}_i \frac{\partial^2 \omega_i}{\partial x_j \partial x_j}. \tag{5}$$

It is interesting, then, to consider this in terms of the logarithm of vorticity magnitude,

$$\frac{d\ln\omega}{dt} = \widehat{\omega}_i S_{ij}\widehat{\omega}_j + \nu\frac{\widehat{\omega}_i}{\omega}\frac{\partial^2 \omega_i}{\partial x_j \partial x_j}. \tag{6}$$

The first term on the right-hand side, $\widehat{\omega}_i S_{ij}\widehat{\omega}_j$, represents vorticity stretching (enstrophy production) by the strain-rate tensor. This paper will focus primarily on this term, using the large-deviation formalism to represent its statistics. The second term represents the effect of viscous forces, preventing the unbounded growth in vorticity magnitude at finite ν.

Complementing Eq. (6) for the vorticity magnitude is the equation for the evolution of the vorticity orientation,

$$\frac{d\widehat{\omega}_i}{dt} = (\delta_{ik} - \widehat{\omega}_i\widehat{\omega}_k)\, S_{kj}\widehat{\omega}_j + \nu\left[(\delta_{ik} - \widehat{\omega}_i\widehat{\omega}_k)\frac{\partial^2 \widehat{\omega}_k}{\partial x_j \partial x_j} + 2\frac{\partial\widehat{\omega}_i}{\partial x_j}\frac{\partial\ln\omega}{\partial x_j}\right]. \tag{7}$$

The first term on the right-hand side represents the rotation/re-alignment of the vorticity due to the strain-rate tensor. This term shows that the strain rate acts to rotate the vorticity

5

toward alignment with the strain-rate eigenvector associated with the largest eigenvalue. Such an alignment is not observed in single-time statistics due to the lack of persistent straining [44], i.e. the vorticity never "catches up" with the strain-rate. However, allowing for a time lag, it has been observed that the vorticity shows statistical bias toward aligning with the eigenvector of the largest eigenvalue of the strain-rate tensor at a previous time along the Lagrangian path [45, 46].

The second term on the right-hand side represents the viscous-tilting effect [22]. In this form, we see that the viscous tilting has contributions from the Laplacian of the vorticity unit vector (projected normal to the unit vector) and from the vorticity curvature tensor[47], $\frac{\partial \widehat{\omega}_i}{\partial x_j}$, acting on the gradient of $\ln \omega$. The vorticity tilting effect is responsible for the difference in Lagrangian evolution between vorticity and infinitesimal material lines that are initialized in alignment with the local vorticity [19].

The focus of this paper is on the statistics of the vorticity stretching term, $\widehat{\omega}_i S_{ij} \widehat{\omega}_j$. The eigenframe of the strain-rate tensor is useful to clarify the connection between the magnitude of the vorticity stretching term and the vorticity orientation dynamics. In this frame it is seen that [38],

$$\widehat{\omega}_i S_{ij} \widehat{\omega}_j = \sum_{i=1}^{3} \Lambda_i \cos^2 \left(\theta_i \right), \tag{8}$$

where Λ_i is the ith eigenvalue of the strain-rate tensor and θ_i is the angle between the vorticity vector and the eigenvector associated with the ith eigenvalue of the strain-rate tensor. Thus, the vorticity stretching can be viewed as a weighted average of the three strain-rate eigenvalues, where the weight of a given eigenvalue is determined by how closely its eigenvector aligns with the vorticity vector being stretched. In this paper, we consider the statistics of the cumulative vorticity stretching along a Lagrangian path using the large deviation formalism.

B. Large Deviation Formalism

According to the large-deviation formalism, which can be traced back to Cramér [48], a sum of N independent and identically-distributed (i.i.d.) random variables, $Y_N = \sum_{i=1}^{N} x_i$, in the limit $N \to \infty$, has the probability density function (PDF) that behaves as

$$p_Y(\xi, N) \sim \exp\left[-N S_y \left(\frac{\xi}{N} \right) \right], \tag{9}$$

6

where S_y is the so-called Cramér function (sometimes also called the entropy or rate function). The Cramér function quantifies the self-similar collapse of the PDF of $y_N = \frac{Y_N}{N}$ to a Dirac delta-function at $\langle x \rangle$. The justification of the large-deviation formalism depends on the additivity of cumulants (cumulant-generating functions) for independent variables, as well as the fact that identically distributed variables share the same cumulant-generating function. With these properties, the cumulants of the sum, Y_N, are equal to N times the cumulants of the independent variables, x_i. The validity of Eq. (9) thus hinges on the linear growth of the cumulants of Y_N with N.

The large-deviation formalism can be extended to applications with the integration over a continuous variable with finite correlation time, $Y(T) = \int\limits_0^T x(t)dt$. Here, the integral can be thought of as a sum of many integrals over sub-intervals, $[t_i, t_i + \Delta t)$, of the full integration interval $[0, T)$, each sub-integral being over a sufficiently large interval that it is independent of the others (and identically distributed assuming stationarity of $x(t)$). In this case, the probability density function of the integral becomes, in the limit $T \to \infty$,

$$p_Y(\xi, T) \sim \exp\left[-TS_y\left(\frac{\xi}{T}\right)\right]. \tag{10}$$

The validity of Eq. (10) hinges on the linear growth of the cumulants of $Y(T)$ with increasing integration time T.

The preceding discussion provides an informal expectation for a large deviation principle to hold. In fact, the application of a large-deviation principle has been extended rigorously well beyond the case of sums of i.i.d. variables. The Gärtner-Ellis theorem [49, 50] gives the existence of a scaled cumulant-generating function as a criterion for the applicability of a large deviation principle. Furthermore, Donsker and Varadhan have provided a rigorous basis large-deviation statistics of general Markovian systems [51–54].

To date, the large-deviation formalism has found many fruitful applications within the study of turbulent flows. It forms the basis for the multifractal theory in three-dimensional turbulence [9–11, 55, 56], where the singularity spectrum $f(\alpha)$ is related to the Cramér function. Large-deviation statistics have been used to digest the results of shell models [57, 58]. It has also been used for passive scalar advection [59], the stretching of polymers [40, 41, 60, 61], the clustering of inertial particles [62, 63], droplet deformation [36], and other applications reviewed by Ref. [64]. Furthermore, it is important for developments in the statistical mechanical description of two-dimensional turbulence [65–68]. Meanwhile,

the large-deviation statistics of FTLEs in two-dimensional turbulence and the impact on vorticity increments was explored [69]. Additionally, the bistability of two-dimensional flows has been investigated using large-deviation statistics [70, 71].

C. Material Lines and Finite-Time Lyapunov Exponents

An infinitesimal material line evolves as

$$\frac{dr_i}{dt} = A_{ij}r_j, \tag{11}$$

along a Lagrangian path. Performing the same decomposition as with the vorticity above, $r_i = r\widehat{r}_i$, this can be decomposed into an equation for the magnitude and an equation for the orientation,

$$\frac{d\ln r}{dt} = \widehat{r}_i S_{ij}\widehat{r}_j, \qquad \frac{d\widehat{r}_i}{dt} = (\delta_{ik} - \widehat{r}_i\widehat{r}_k)S_{kj}\widehat{r}_j + \Omega_{ij}\widehat{r}_i. \tag{12}$$

For material lines, integrating the first part of Eq. (12) results in

$$\Gamma(T) = \ln\left(\frac{r(T)}{r(0)}\right) = \int_0^T \widehat{r}_i S_{ij}\widehat{r}_j dt. \tag{13}$$

Furthermore, given the finite correlation time of the strain-rate along Lagrangian paths[72, 73], proportional to the Kolmogorov time-scale τ_η, and given the passive nature of the material line (i.e. S_{ij} does not depend on r), the application of the large-deviation formalism is quite straight-forward. In this case, the finite-time Lyapunov exponent (FTLE) [74–76], is intimately related to this result,

$$\gamma(T) \equiv \frac{1}{T}\ln\left(\frac{r(T)}{r(0)}\right) = \frac{1}{T}\int_0^T \widehat{r}_i S_{ij}\widehat{r}_j dt. \tag{14}$$

Accordingly, the PDF of FTLEs evolves as

$$p_\gamma(g,T) \sim \exp\left(-TS_\gamma(g)\right), \tag{15}$$

where g is the sample space variable for the FTLE. Cramér functions, S_γ, of the largest FTLE have been computed by Bec et al. [63] and for the entire FTLE spectrum (including for joint-statistics) by Johnson and Meneveau [35] for the case of isotropic turbulence.

8

D. Vorticity

Seeing that a large-deviation principle has been shown for cumulative material deformation along Lagrangian paths, it is interesting to seek one also for cumulative Lagrangian vorticity stretching. A large-deviation principle for vorticity stretching would allow a more detailed comparison with material line stretching in terms of the Cramér function, which describes the self-similar behavior of the cumulative stretching PDF along Lagrangian paths. The existence of a large-deviation principle in the case of Lagrangian material deformation provides a strong rationale for expecting one to hold in the case of Lagrangian vorticity stretching, although a rigorous proof is not available and so it must be shown empirically. The first task in this paper is to verify that the cumulative vorticity stretching term indeed behaves in such a way as to support the application of the large deviation formalism. Secondly, we seek to determine the integration time T needed to allow for such behavior to take hold.

As already stated, this paper seeks to study only the vorticity stretching term in the vorticity evolution equation, without considering any details of the viscous term. Thus neglecting the viscous term, we define an increment of $\ln \omega$,

$$\Gamma_\omega(T) \equiv \Delta_T(\ln \omega) = \ln \left(\frac{\omega(T)}{\omega(0)} \right) = \int_0^T \widehat{\omega}_i S_{ij} \widehat{\omega}_j dt, \tag{16}$$

such that there is an analog to the FTLE for the vorticity stretching,

$$\gamma_\omega(T) \equiv \frac{\Gamma_\omega(T)}{T} = \frac{1}{T} \ln \left(\frac{\omega(T)}{\omega(0)} \right) = \frac{1}{T} \int_0^T \widehat{\omega}_i S_{ij} \widehat{\omega}_j dt. \tag{17}$$

Because the viscous term has been discarded, comparison of statistical behavior between γ_ω and that of the FTLEs, especially the largest FTLE γ_1, allows for an exploration of the differences between the stretching of vorticity and material lines by strain-rates in turbulence.

A useful quantity is the scaled cumulant-generating function (which is analogous to the generalized Lyapunov exponent[76]),

$$L_{\gamma_\omega}(q) = \lim_{T \to \infty} \frac{1}{T} \ln \left\langle \exp \left(q \gamma_\omega T \right) \right\rangle, \tag{18}$$

which exists only if the cumulant-generating function for $\Gamma_\omega(T)$ grows linearly in time. If this cumulant-generating function, $\ln \left\langle \exp \left(q \gamma_\omega T \right) \right\rangle$, can be shown to grow linearly with time,

9

the slope as a function of q gives the generalized Lyapunov exponent, $L(q)$. Furthermore, casting the PDF in the form of Eq. (15) to compute the ensemble average in Eq. (18), and using steepest-descent integration in the $T \to \infty$ limit, it results that $L(q)$ is the Legendre transform of S_{γ_ω},

$$L_{\gamma_\omega}(q) = \sup_g \left[qg - S_{\gamma_\omega}(g) \right]. \tag{19}$$

For the present purposes, the linear growth of the cumulant-generating function (i.e. the existence of $L_{\gamma_\omega}(q)$) is considered sufficient evidence that the PDF of γ_ω behaves according to Eq. (15). Direct numerical simulations of forced isotropic turbulence in a periodic domain can be used to test the hypothesis that the vorticity stretching term should behave in this way.

III.   NUMERICAL METHODS

In this section, the numerical methods applied in this study are briefly introduced. This study uses a direct numerical simulation dataset for gathering statistics for isotropic turbulence, and performs Lagrangian particle tracking with velocity gradient extraction to evaluate important terms for the vorticity evolution equation.

The Johns Hopkins Turbulence Databases (JHTDB) isotropic dataset [77, 78] is used for the turbulence statistics reported in this paper. This dataset was constructed from a pseudo-spectral simulation of Eq. (1) in a 2π periodic cube with 1024^3 resolution. The simulation used the 2nd-order Adams-Bashforth scheme for time advancement and $2\sqrt{2}/3$ truncation with random phase shift for de-aliasing. Important parameters for the simulation are given in Table I.

TABLE I. Numerical details for JHTDB (Refs. 77 and 78) simulation used in this paper.

N	Re_λ	ϵ	ν	η	τ_η	Δt (simulation)	Δt (saved)	T
1024^3	433	0.928	1.85e-04	2.87e-03	0.045	2e-04	2e-03	2.048

The simulation code wrote the full velocity and pressure fields to disk every 10 time steps for storage on the public database cluster. In total, 1024 consecutive snapshots of the entire fields are stored, allowing for the tracking of Lagrangian trajectories for up to $45\tau_\eta$

with temporal resolution of $\Delta t = \tau_\eta/22$. The public database functionality provides built-in Lagrangian particle tracking [79].

For this paper, ensembles of 64k particles were tracked using the 2nd order predictor-corrector method with cubic Hermite interpolation in time and 6th order Lagrange interpolation in space. For the initial distribution of particles, the $(2\pi)^3$ domain was divided into 1000 cubes of equal size $(\pi/5)^3$. Within each sub-cube, 64 particle trajectories were initialized at random positions, selected from a uniform spatial distribution along each coordinate. In this way, a uniform coverage of the domain was ensured within a randomized initialization procedure. Predictor-corrector steps were taken with a time-step of $\frac{1}{5}^{th}$ of the storage time step.

At each time step, velocity gradients were extracted from the dataset using 4th order finite-differencing with 4th order Lagrangian interpolation in space and cubic Hermite interpolation in time. The cumulative vorticity stretching along each trajectory, Eq. (16), was computed using the midpoint rule for numerical integration.

IV.   THE CRAMÉR FUNCTION FOR VORTICITY STRETCHING

In this section, the method for constructing the Cramér function from the Lagrangian vorticity stretching data is presented. The resulting Cramér function for vorticity stretching in isotropic turbulence is shown.

A.   Legendre Transform Method

In previous work, Johnson and Meneveau [35] compared two methods for constructing the Cramér function for material deformation: (i) histogram-based construction of the PDF and finite-size compensation via vertical shift of the Cramér function, (ii) moment-based construction of the generalized Lyapunov exponent with (inverse) Legendre transform to construct the Cramér function. The Legendre transform method proved superior in that case and is adopted here. Another advantage of this method is the explicit evaluation of the cumulant-generating function, which is useful for verifying the applicability of the large-deviation formalism to vorticity stretching. Below, the method is briefly outlined before presenting results.

11

The first step in the moment-based method for constructing the Cramér function is to compute the generalized Lyapunov exponent, $L_{\gamma_\omega}(q)$, given by Eq. (18). To construct $L_{\gamma_\omega}(q)$, the cumulant-generating function, $\ln \langle \exp(q\gamma_\omega T) \rangle$, is calculated as a function of q and T. The applicability of the large-deviation formalism requires the results to asymptotically $(T \to \infty)$ grow linearly with integration time. The cumulant-generating function is plotted for sample values of $-1 < q < 1$ as a function of integration time in Fig. 1. In this range, the linear growth in time is a striking feature of the results.
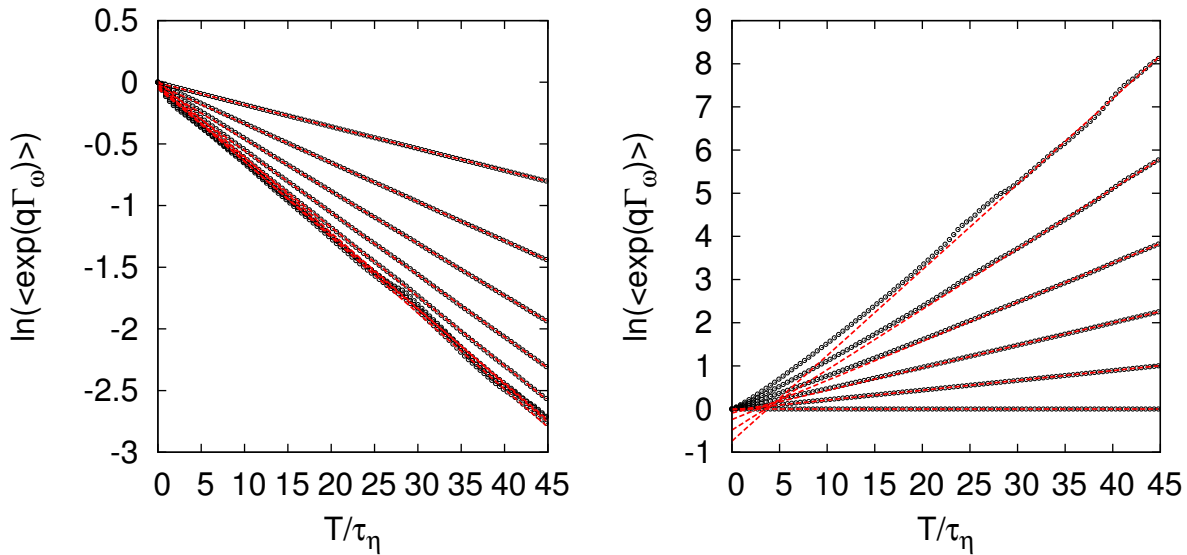

FIG. 1. The cumulant-generating function for the cumulative vorticity stretching, $\Gamma_\omega = \gamma_\omega T$, for (a) $q = -1.6, -1.4, -1.2, -1.0, -0.8, -0.6, -0.4, -0.2$, and (b) $q = 0, 0.2, 0.4, 0.6, 0.8, 1.0$. Symbols represent numerical values from the dataset and dashed-lines represent linear curve-fits for the $30\tau_\eta < T < 45\tau_\eta$ range.

On the basis of the evidence shown in Fig. 1, it is concluded that the required behavior for the applicability of the large-deviation formalism is seen for vorticity stretching, even at relatively small integration times $\sim 30\tau_\eta$. The slopes of the curve fits (shown as dotted lines in Fig. 1) then represent the generalized Lyapunov exponent at a given q. Using a linear regression procedure for $-3 < q < 3$ with uniform discretization of $\Delta q = 0.02$, the generalized Lyapunov exponent is constructed and shown in Fig. 2 for five different ensembles of $64k$ particles each. The linear regression was performed only on the interval $30\tau_\eta < T < 45\tau_\eta$. A specified threshold on the 95% confidence interval, computed from the

standard error of the regression analysis, was used to determine the range over which the curve fits were reliable. Points with standard error above this threshold were removed.
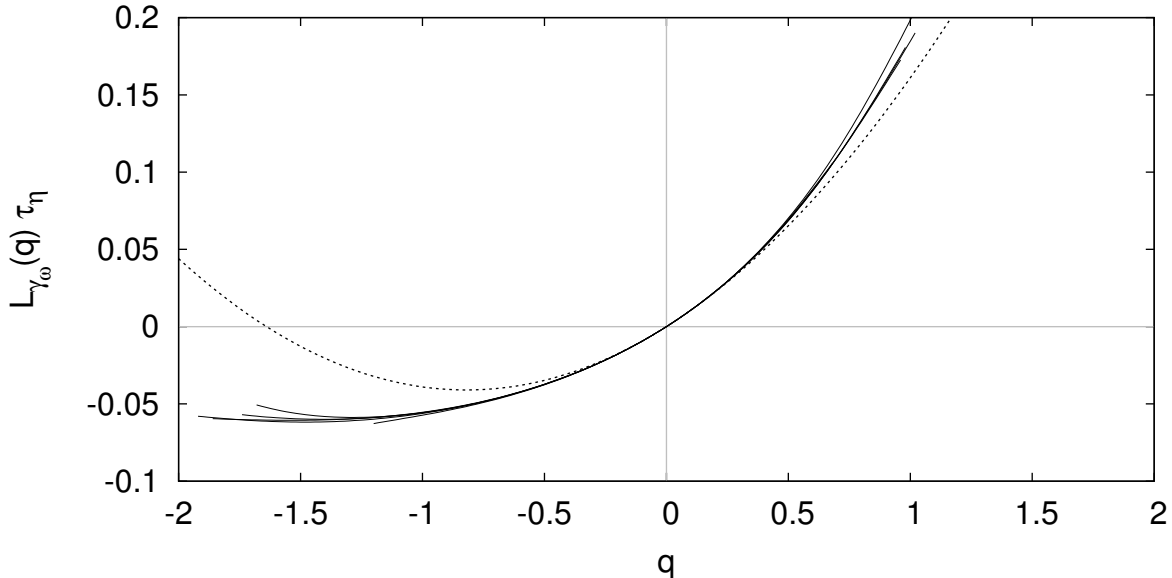

FIG. 2. The generalized Lyapunov exponents for the vorticity stretching from five different $64k$ Lagrangian particle ensembles. The dashed line represents a parabolic curve fit in the region of $q = 0$.

The spread of the five curves in this figure, especially noticeable in the tails, is indicative of the statistical convergence error. The curves pass through the origin as expected and near the origin can be approximated by a truncated Taylor expansion[76],

$$L_{\gamma_\omega}(q) \approx \lambda_\omega q + \frac{1}{2}\Delta_\omega q^2. \tag{20}$$

The slope at the origin, $L'_{\gamma_\omega}(0) = \lambda_\omega = \langle \widehat{\omega}_i S_{ij} \widehat{\omega}_j \rangle \approx 0.100/\tau_\eta$, represents the average vorticity stretching and is analogous to the Lyapunov exponent of Lagrangian trajectories in the context of material line stretching. The curvature at the origin, $L''_{\gamma_\omega}(0) = \Delta_\omega \approx 0.122/\tau_\eta$, gives a measure of the strength of fluctuations in cumulative stretching about the mean. This parabolic approximation is shown in Fig. 2 as a dashed line.

As given by Eq. (19), the generalized Lyapunov exponent is the Legendre transform of the Cramér function. For a known generalized Lyapunov exponent, the inverse Legendre transform can be used to recover the (convex hull of the) Cramér function,

$$S_{\gamma_\omega}(g) = \sup_q \left[gq - L_{\gamma_\omega}(q) \right]. \tag{21}$$

13

The inverse Legendre transform is performed numerically, for a given g-q pair,

$$g = L'_{\gamma_\omega}(q), \qquad S_{\gamma_\omega}(g) = qL'_{\gamma_\omega}(q) - L_{\gamma_\omega}(q), \tag{22}$$

using second-order central differencing for the derivative of the generalized Lyapunov exponent.

Figure 3 shows the resulting Cramér function for the vorticity stretching term. The minimum of the Cramér function is $S_{\gamma_\omega}(\lambda_\omega) = 0$. A truncated Taylor expansion about the minimum gives a parabola,

$$S_{\gamma_\omega}(g) \approx \frac{(g - \lambda_\omega)^2}{2\Delta_\omega}, \tag{23}$$

which is the Legendre transform of the parabolic generalized Lyapunov exponent given in Eq. (20). The dashed line in Fig. 3 shows this approximation. Substitution of Eq. (23) into Eq. (15) yields Gaussian statistics, that is, the Gaussian toward which the central-limit theorem predicts that the PDF is approaching for $T \to \infty$.
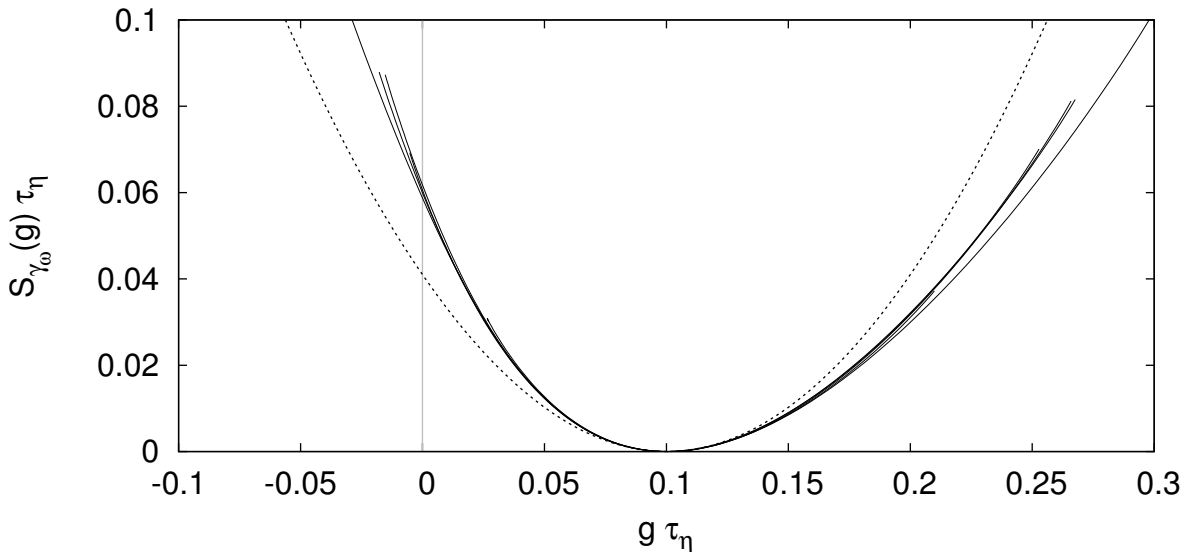

FIG. 3. The Cramér function for the vorticity stretching from five different $64k$ Lagrangian particle ensembles. The differences between the five different ensembles illustrate the extent of uncertainty from statistical convergence. The symbol g is used for the probability space variable of γ_ω and both axes are non-dimensionalized by the Kolmogorov timescale τ_η. The gray vertical line indicates $\gamma_\omega = 0$. The dashed line represents a parabolic curve fit to the Cramér function near the minimum.

14

B. Comparison with FTLE Spectrum

In §II, an analogy was drawn between the behavior of vorticity along Lagrangian trajectory and the behavior of material lines. Specifically in the context of large deviation statistics, the quantity γ_ω was introduced to quantify the cumulative stretching of vorticity by the strain-rate tensor along Lagrangian paths. This quantity is directly analogous to the finite-time Lyapunov exponents (FTLE) of Lagrangian trajectories, γ_i with $i = 1, 2, 3$, which characterize the cumulative deformation of a fluid volume by the strain-rate tensor. Specifically, γ_1 can be used to investigate material line stretching and $\gamma_1 + \gamma_2$ for material surface area stretching. It is of interest, therefore, to compare the large deviation statistics of cumulative vorticity stretching with those of the FTLEs as a way of exploring similarities and differences in vorticity and material line behavior in turbulence.

It is known that vorticity tends to align most readily with the strain-rate eigenvector corresponding to the intermediate eigenvalue[14], Λ_2, while material lines tend to align more with the eigenvector corresponding to the largest eigenvalue[19], Λ_1. As a result, the mean material line stretching, $\langle \hat{r}_i S_{ij} \hat{r}_j \rangle$, is larger than the mean vorticity stretching, $\langle \hat{\omega}_i S_{ij} \hat{\omega}_j \rangle$.

For material lines, the first term in Eq. (12), $(\delta_{ik} - \hat{r}_i \hat{r}_k) S_{kj} \hat{r}_j$, shows that the strain-rate tends to tilt material lines in the direction of the strongest strain. Perfect alignment does not occur, in fact, because of the impact of vorticity on the material line, $\Omega_{ij} \hat{r}_j$, and the fact that the strain-rate eigenvectors are moving targets, being themselves rotated by the vorticity and non-local pressure Hessian [80]. For vorticity, Eq. (7), the $\Omega_{ij} \hat{\omega}_j$ term vanishes and is replaced by the viscous tilting terms. The tendency of the strain-rate to rotate vorticity toward its largest eigenvalue remains. A vital difference is the active feedback that the vorticity has on the strain-rate evolution (as opposed to passive material lines). This appears to be the key ingredient in the vorticity's alignment bias toward the second largest eigenvalue[19].

The ratio of Lyapunov exponents (the average stretching of mutually orthogonal material lines) in isotropic turbulence is approximately $\lambda_1 : \lambda_2 : \lambda_3 \approx 4 : 1 : -5$ [35, 63]. In Fig. 4, the Cramér function for cumulative vorticity stretching is compared with the Cramér functions for the Lyapunov spectrum (see [35] for details). Bec et al. [63] reported a leading Lyapunov exponent of $\lambda_1 \tau_\eta \approx 0.14$ while Johnson and Meneveau [35] found $\lambda_1 \tau_\eta \approx 0.125$ after correcting for finite integration time effects (with S_{γ_1} evaluated up to $45\tau_\eta$ it is slightly

lower, i.e. $\lambda_1 \tau_\eta \approx 0.114$, as shown in Fig. 4). For vorticity, the present results show mean stretching, $\lambda_\omega \tau_\eta = \langle \widehat{\omega}_i S_{ij} \widehat{\omega}_j \rangle = 0.10$, which is significantly lower than that of the mean stretching for material lines. Guala et al. [19] measured $\langle \widehat{\omega}_i S_{ij} \widehat{\omega}_j \rangle$ and $\langle \widehat{r}_i S_{ij} \widehat{r}_j \rangle$ for short evolution times up to $6\tau_\eta$, concluding that the material lines had significantly stronger stretching. Indeed, this is easy to understand, since the vorticity tends to preferentially align with the second-largest strain-rate eigenvalue, while material lines tend to tilt towards the largest one. However, here it is shown that the mean vorticity stretching rate greatly exceeds that of the second-largest FTLE, and is much closer to λ_1 than $\lambda_2 \approx 0.03/\tau_\eta$.
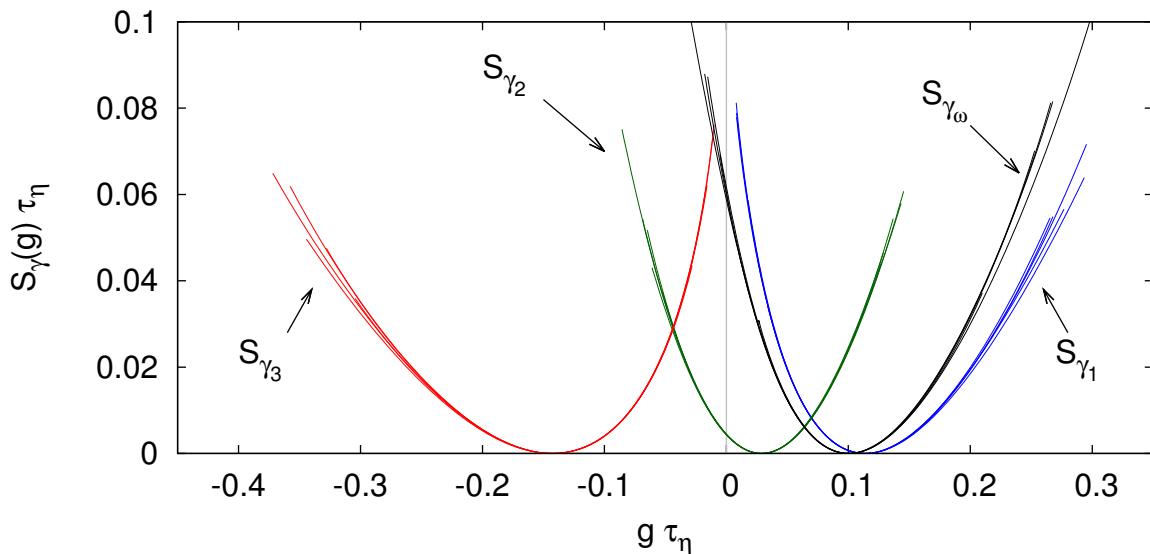

FIG. 4. Comparison of the Cramér function for vorticity stretching with the marginal Cramér functions for the finite-time Lyapunov exponents[35]. Each Cramér function was measured from five separate ensembles of $64k$ Lagrangian particles each in order to demonstrate the level of statistical convergence uncertainty. The symbol g is used for the probability space variable of γ and both axes are non-dimensionalized by the Kolmogorov timescale τ_η. The gray vertical line indicates $\gamma = 0$.

The width of the Cramér function of cumulative vorticity stretching is visually very similar to that of the largest FTLE. To quantify the behavior of these Cramér functions, the derivatives of the generalized Lyapunov exponent at the origin are used. As apparent from the relation of Eq. (18) to the cumulant-generating function of $\Gamma = \gamma T$, these derivatives represent the growth rate of cumulants, e.g. of the integrated vorticity stretching, $\Gamma_\omega =$

$\int_0^T \widehat{\omega}_i S_{ij} \widehat{\omega}_i dt$. In addition to mean, $\lambda T = L'(0)T$, and variance, $\Delta T = L''(0)T$, the deviation from Gaussian statistics can be quantified by the skewness,

$$\mathcal{S} = \frac{L'''(0)T}{(L''(0)T)^{3/2}} = \frac{L'''(0)\tau_\eta}{(L''(0)\tau_\eta)^{3/2}} \left(\frac{T}{\tau_\eta}\right)^{-1/2}, \tag{24}$$

and excess kurtosis,

$$\mathcal{K} - 3 = \frac{L^{(4)}(0)T}{(L''(0)T)^2} = \frac{L^{(4)}(0)\tau_\eta}{(L''(0)\tau_\eta)^2} \left(\frac{T}{\tau_\eta}\right)^{-1}. \tag{25}$$

Note that, in agreement with the central-limit theorem, the skewness and excess kurtosis (and all higher-order cumulants) are decaying to zero at $T \to \infty$. The large-deviation formalism gives a means for computing the rate at which they decay. Table II shows these cumulant values for three of the curves in Fig. 4. The derivatives were evaluated using fourth-order polynomial curve fits to $L(q)$ near $q = 0$ and averaged over each of the five ensembles. It is apparent from this analysis that the cumulative vorticity stretching statistics behave more similarly to γ_1 than γ_2. The cumulative vorticity stretching and largest FTLE have much larger deviations from Gaussian statistics (skewness and excess kurtosis) than the second-largest FTLE for a given integration time.

TABLE II. Comparison of first four cumulants for the vorticity stretching with those of the first two FTLEs. The asterisk denotes that the value is corrected for finite integration time effects, see [35] for more details.

	$\lambda\tau_\eta$	$\Delta\tau_\eta$	$\mathcal{S}\left(\frac{T}{\tau_\eta}\right)^{1/2}$	$(\mathcal{K}-3)\left(\frac{T}{\tau_\eta}\right)$
γ_1	0.125*	0.145	4.8	30
γ_ω	0.100	0.122	3.6	18
γ_2	0.029	0.098	0.93	2.7

Physically speaking, the intermediate FTLE, γ_2, can be thought of as the cumulative stretching of material lines constrained to be perpendicular to the most stretched material line. Perhaps the most intuitive feel for the significance of γ_2 is to think of cumulative material surface area stretching as $\gamma_1 + \gamma_2$. The similarity between γ_ω and γ_1 is *relative* to the comparison of γ_ω with γ_2 in a statistical sense and should not be seen to overshadow the important differences between vorticity stretching and material line stretching but only

to put them in perspective. For example, while vorticity stretching is on average less than material line stretching, it is still much greater than the average stretching in the plane perpendicular to material lines.

C.   Comparison with Strain-Rate Eigenvalue Statistics

In order to emphasize the effect of preferential alignment of vorticity with the second-largest strain-rate eigenvalue, a Cramér function can be constructed for a vector always in perfect alignment with a given strain-rate eigenvalue. This artificial Cramér function does not reflect any physical dynamics, but rather the hypothetical dynamics of vorticity magnitude if perfect alignment with any of the eigenvectors was maintained. Two such Cramér functions, one for the largest eigenvalue Λ_1 and one for the second-largest eigenvalue Λ_2, are plotted in Fig. 5 alongside the Cramér function for cumulative vorticity stretching. It is clear that the Cramér function for vorticity stretching is much closer to that of perfect alignment with Λ_2 rather than Λ_1, which is consistent with the observed preferential alignment of the vorticity vector.
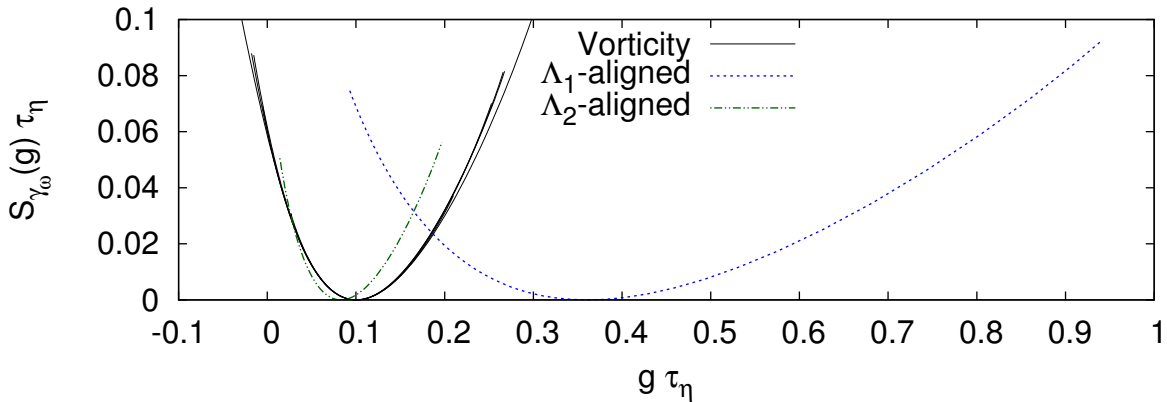

FIG. 5. Comparison of the Cramér function for vorticity stretching with the hypothetical Cramér functions if perfect alignment with the largest or second-largest strain-rate eigenvalues was maintained throughout the dynamics.

18

V. A MODEL KRAMERS-MOYAL EQUATION FOR THE VORTICITY MAGNITUDE

In this section, an application of the above statistical characterization of vorticity stretching to a model for the vorticity magnitude PDF is described. Some of the assumptions of the model are justified by appealing to results from DNS of forced isotropic turbulence. The vorticity magnitude PDF is defined for a statistical ensemble of Lagrangian trajectories, so that the Lagrangian evolution of the vorticity described in the previous sections is the relevant dynamical input to the statistical equations. In addition, the free parameters of the model are prescribed using statistics from DNS. While progress in solving the full model has so far proved difficult, the results of the model for a parabolized Cramér function are presented.

A. PDF Closure Using Conditional Means

The goal of this section is to model the statistics of vorticity magnitude using Eq. (6). To appreciate this goal, first consider the direct approach to constructing the evolution equation for the PDF. Following a similar procedure as Wilczek and Friedrich [81] (i.e. following Lundgren[82], Monin[83], and Novikov[84] with closure introduced through conditional means), the PDF of $\ln \omega$ can be written in terms of the fine-grained PDF,

$$p_{\ln \omega}(\chi, t) = \langle \delta(\ln \omega(t) - \chi) \rangle . \tag{26}$$

Differentiating in time and using conditional mean closure,

$$\frac{\partial p_{\ln \omega}}{\partial t} = -\frac{\partial}{\partial \chi} \left\langle \frac{d \ln \omega}{dt} \delta(\ln \omega(t) - \chi) \right\rangle = -\frac{\partial}{\partial \chi} \left(\left\langle \frac{d \ln \omega}{dt} \middle| \ln \omega = \chi \right\rangle p_{\ln \omega} \right), \tag{27}$$

and substituting Eq. (6) on the right-hand side yields,

$$\frac{\partial p_{\ln \omega}}{\partial t} = -\frac{\partial}{\partial \chi} \left[\left(\langle \widehat{\omega}_i S_{ij} \widehat{\omega}_j | \ln \omega = \chi \rangle + \nu \left\langle \frac{\widehat{\omega}_i}{\omega} \frac{\partial^2 \omega_i}{\partial x_j \partial x_j} \middle| \ln \omega = \chi \right\rangle \right) p_{\ln \omega} \right]. \tag{28}$$

Solving for the stationary PDF, $\frac{\partial p_{\ln \omega}}{\partial t} = 0$, the constant of integration vanishes due to $p_{\ln \omega} \to 0$ as $\ln \omega \to \infty$, resulting in the requirement,

$$\langle \widehat{\omega}_i S_{ij} \widehat{\omega}_j | \ln \omega = \chi \rangle = -\frac{\nu}{\omega} \left\langle \widehat{\omega}_i \frac{\partial^2 \omega_i}{\partial x_j \partial x_j} \middle| \ln \omega = \chi \right\rangle . \tag{29}$$

19

That is, the conditional mean stretching must equal the conditional mean viscous relaxation at every point in probability space for $\ln\omega$. While this is a helpful constraint on the conditional means, it provides no prescription for finding the stationary distribution $p_{\ln\omega}$.

A useful manipulation of the above equation for finding the stationary PDF is found by invoking the fact that for homogeneous turbulence, the vorticity PDF is independent of spatial coordinates, so its Laplacian is zero[81],

$$0 = \frac{\partial^2 p_{\ln\omega}}{\partial x_j \partial x_j} = -\frac{\partial}{\partial\chi}\left(\left\langle \left.\frac{\partial^2 \ln\omega}{\partial x_j \partial x_j}\right| \ln\omega = \chi\right\rangle p_{\ln\omega}\right) + \frac{\partial^2}{\partial\chi^2}\left(\left\langle \left.\frac{\partial \ln\omega}{\partial x_j}\frac{\partial \ln\omega}{\partial x_j}\right| \ln\omega = \chi\right\rangle p_{\ln\omega}\right).$$
(30)

With the help of Eqs. (6) and (30), the evolution equation for $p_{\ln\omega}$, Eq. (28), can be rewritten as

$$\frac{\partial p_{\ln\omega}}{\partial t} = -\frac{\partial}{\partial\chi}\left[\left(\langle\widehat{\omega}_i S_{ij}\widehat{\omega}_j| \ln\omega = \chi\rangle + \nu\left\langle\left.\frac{\partial \ln\omega}{\partial x_j}\frac{\partial \ln\omega}{\partial x_j} - \frac{\partial\widehat{\omega}_i}{\partial x_j}\frac{\partial\widehat{\omega}_i}{\partial x_j}\right| \ln\omega = \chi\right\rangle\right) p_{\ln\omega}\right]$$
$$- \nu\frac{\partial^2}{\partial\chi^2}\left(\left\langle\left.\frac{\partial \ln\omega}{\partial x_j}\frac{\partial \ln\omega}{\partial x_j}\right| \ln\omega = \chi\right\rangle p_{\ln\omega}\right). \quad (31)$$

Indeed, this expression is analogous to one obtained by Wilczek and Friedrich[81] for a single component of the vorticity. Wilczek and Friedrich[81] solved their equation and numerically evaluated two conditional averages from DNS, showing that such an approach can exactly reconstruct the PDF for a single component of vorticity. The present goal is to introduce a model which incorporates the statistical information from the Cramér function of vorticity stretching to reconstruct the vorticity magnitude PDF.

B.   Analogy with Polymers

We first invoke an analogy between vorticity stretching and polymer stretching in turbulence. Representing the polymer with a bead-spring model, with vector ρ_i signifying the displacement between the two ends of the polymer, the polymer equation along a Lagrangian path is modelled with

$$\frac{d\rho_i}{dt} = A_{ij}\rho_j - f(|\rho|)\frac{\rho_i}{|\rho|},$$
(32)

where $f(|\rho|)$ represents the elastic restoration force of the polymer [41]. For the Oldroyd-B model, the restoration force is that of a linear spring, $f(|\rho|) = \frac{|\rho|}{\tau_p}$, where τ_p is the relaxation time of the polymer [40, 41]. The Oldroyd-B model allows infinite extension of the

polymer, and therefore a popular extension is the non-linear FENE-P model [85]. On the decomposition $\rho_i = \rho \widehat{\rho}_i$, the equations become,

$$\frac{d \ln \rho}{dt} = \widehat{\rho}_i S_{ij} \widehat{\rho}_j - \frac{f(\rho)}{\rho}, \qquad \frac{d \widehat{\rho}_i}{dt} = (\delta_{ik} - \widehat{\rho}_i \widehat{\rho}_k) S_{kj} \widehat{\rho}_j + \Omega_{ij} \widehat{\rho}_j. \tag{33}$$

These equations resemble those of the material line, Eq. (12), except that they now contain a relaxation term to prevent unbounded growth of the polymer.

Comparison with Eqs. (6) and (7) reveals three differences between the evolution equations for polymers and vorticity. First, while both the vorticity and polymer stretching are resisted by a second term that acts to prevent unbounded growth, the relaxation term in the polymer length equation is due to the properties of the polymer, whereas the viscous term in the vorticity equation is a function of the flow in the neighborhood of the point (and therefore, much more challenging to model). Second, there is no viscous tilting in the equation for the polymer orientation evolution, because the polymer relaxation always acts along the polymer axis. Third, the polymer can be rotated by the vorticity, whereas the vorticity cannot rotate itself: $\Omega_{ij} \widehat{\omega}_j = 0$.

Perhaps the most important difference, however, is not obvious in this comparison: how the vorticity and polymers affect the strain-rate that is stretching them. Both the vorticity and polymers can have a back-reaction on the flow, though the details of the two-way coupling vary. However, especially below the coil-stretch transition, the polymer can be approximately modelled as a passive entity [40, 41]. There is no similar regime for the vorticity in which a passive treatment is a good approximation.

For polymers, under the assumption that the polymer has negligible influence on the flow (i.e. on S_{ij}), the integration of the first part of Eq. (33) gives

$$\ln \left(\frac{\rho(T)}{\rho(0)} \right) = \int_0^T \left(\widehat{\rho}_i S_{ij} \widehat{\rho}_j - \frac{f(\rho)}{\rho} \right) dt. \tag{34}$$

Because the orientation of the polymer, Eq. (33), follows the same equation as the orientation of the material line, Eq. (12), the statistics of $\widehat{\rho}_i S_{ij} \widehat{\rho}_j$ are identical in these cases, and the Cramér function for material lines can be directly used. For this reason, the large-deviation formalism has been found useful for studying polymer length distributions [40, 41, 60].

C. Modeling Approximations

The qualitative resemblance of vorticity stretching statistics to material line stretching in Fig. 4, despite the fact that the vorticity plays an active role in turbulent dynamics, motivates the attempt to model and approximate the vorticity as a passive vector with relaxation. This is the first and most drastic modeling approximation, removing the effect of the vorticity on the strain-rate. Statistically, this effectively removes the dependence of the conditional mean vorticity stretching on the vorticity magnitude, i.e. $\langle \widehat{\omega}_i S_{ij} \widehat{\omega}_j | \ln \omega = \chi \rangle = \langle \widehat{\omega}_i S_{ij} \widehat{\omega}_j \rangle = \lambda$. While this approach does neglect the effect of vorticity/strain-rate coupling which makes the vorticity stretching rate directly dependent on the instantaneous value of vorticity magnitude, the effects of vorticity/strain-rate coupling on the statistics of vorticity stretching fluctuations are preserved by using the appropriate Cramér function.

With the mean of the vorticity stretching thus fixed as the minimum of the Cramér function, the model is constructed to incorporate the rest of the Cramér function into information about fluctuations in vorticity stretching. To accomplish this, the second modeling approximation proposes an intermediate time-scale, $\tau_S \ll T \ll \tau_\Omega$, at which the vorticity stretching can be modeled as a stochastic noise with statistics prescribed by the Cramér function shown previously in this paper. This approximation can be thought of in the same vein as the Kraichnan ensemble[86], in which rapid velocity field fluctuations are modeled statistically as white-in-time stochastic terms. Indeed, the auto-correlation for vorticity has been found to be significantly longer than that of the strain-rate along Lagrangian trajectories in isotropic turbulence [72, 73], though perhaps not enough to justify this model.

Finally, the model treats the viscous relaxation as deterministic. In other words, the viscous relaxation term in Eq. (5) is modeled as, $\nu \, \widehat{\omega}_i \frac{\partial^2 \omega_i}{\partial x_j \partial x_j}\Big|_{\omega=w} \approx -f(w)$, where $f(w)$ is a deterministic function. In particular, the deterministic relaxation is set to be equal to the conditional mean given a particular value of the vorticity magnitude,

$$f(w) = -\nu \left\langle \widehat{\omega}_i \frac{\partial^2 \omega_i}{\partial x_j \partial x_j} \,\middle|\, \omega = w \right\rangle. \tag{35}$$

With this model for the relaxation, the vorticity evolution along a Lagrangian path in dimensionless form, from Eq. (6), becomes,

$$\frac{d \ln(\omega \tau_\eta)}{d \left(t/\tau_\eta \right)} = \widehat{\omega}_i S_{ij} \tau_\eta \widehat{\omega}_j - \frac{f(\omega) \tau_\eta^2}{\omega \tau_\eta}, \tag{36}$$

22

which is identical to Eq. (33) for the polymer length. The difference between vorticity and polymer length, however, is the difference in the relaxation functions.

Such a function can be measured from DNS results of forced isotropic turbulence. We note that it is possible to measure the right-hand side of Eq. (35) directly, or indirectly using Eq. (29). Because evaluation of these statistics from the JHTDB isotropic dataset utilizes finite-differences in physical space (as opposed to spectral differentiation), it is preferable to measure the conditional mean of the viscous term indirectly using Eq. (29). The indirect calculation requires only first derivatives of the velocity field (i.e. the strain-rate) while the direct calculation requires third derivatives of the velocity field (i.e. Laplacian of vorticity).

Figure 6 shows the results as computed from the JHTDB isotropic dataset, using $\widehat{\omega}_i S_{ij} \widehat{\omega}_j$ computed at 100 million points using an 8th-order finite difference. The scatter in the conditional mean at large $\omega \tau_\eta$ is due to lack of statistical convergence. It is found that a power law functional form for the deterministic relaxation function,

$$f(\omega)\tau_\eta^2 = A \ (\omega \tau_\eta)^n, \tag{37}$$

provides an excellent fit to the numerical results. The best fit of this form is shown in Fig. 6a, with $A = 0.129$, $n = 1.462$ (we remark that this fitted value is very close to 3/2). Figure 6b shows the conditional coefficient of variance (conditional standard deviation divided by conditional mean) for the viscous relaxation term. For increasing vorticity magnitude, the conditional coefficient of variance decreases toward zero, meaning that the viscous relaxation behaves increasingly like a deterministic variable for large vorticity magnitudes (the tail of the PDF). This helps to justify one of the modelling approximations.

With these modeling assumptions, we have a stochastic model for the Lagrangian vorticity magnitude, here given in dimensionless form,

$$d \ln(\omega \tau_\eta) = \{\lambda \tau_\eta - A \ \exp[(n-1) \ln(\omega \tau_\eta)]\} \frac{dt}{\tau_\eta} + d\mathcal{W}, \tag{38}$$

where $d\mathcal{W}$ represents a stochastic forcing term with zero mean and increment statistics in agreement with the large-deviation statistics of the vorticity stretching fluctuations. Approximating the vorticity stretching Cramér function as a parabola, the statistics become Gaussian and $d\mathcal{W} = \sqrt{\Delta \tau_\eta} dW$, where Δ is the width of the Cramér function and dW represents a Wiener process.
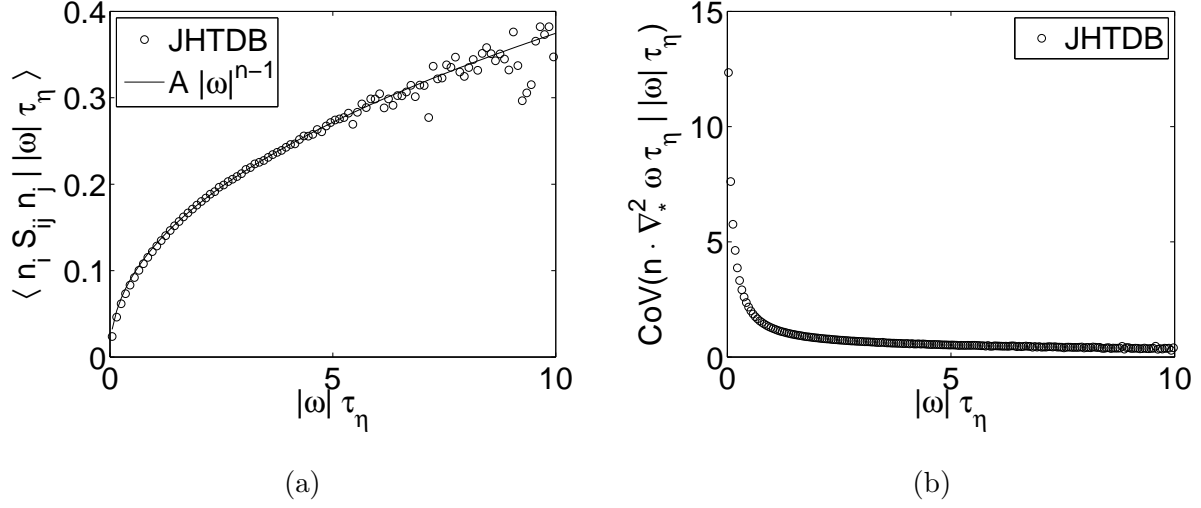
23

FIG. 6. (a) The conditional mean, Eq. (35), as computed indirectly from the strain-rate using Eq. (29). Also shown is a power-law curve fit of the form, Eq. (37) for the interval $2 < |\omega|\tau_\eta < 6$, with $A = 0.129$, $n = 1.462$. (b) The conditional coefficient of variation (standard deviation/mean) of the relaxation term.

D. Kramers-Moyal Coefficients

The above model is a Markovian stochastic model, for which we seek a PDF evolution equation in the form of the Kramers-Moyal equation for $p_{\ln \omega}(\chi, T)$, (see Pope[3] Appendix J),

$$\frac{\partial p_{\ln \omega}}{\partial T} = \sum_{m=1}^{\infty} \frac{(-1)^m}{m!} \frac{\partial^m}{\partial \chi^m} \left(B_m p_{\ln \omega} \right), \tag{39}$$

where the Kramers-Moyal coefficients are given by,

$$B_m(\chi) = \lim_{T \to 0} \frac{1}{T} \left\langle \Delta_T(\ln \omega)^m \,|\, \ln \omega = \chi \right\rangle, \tag{40}$$

and where the increment of $\ln \omega$ is

$$\Delta_T(\ln \omega) = \ln \omega(t + T) - \ln \omega(t). \tag{41}$$

Applying this approach to Lagrangian vorticity evolution, it is clear from Eq. (36) that the vorticity increments are given by

$$\Delta_T(\ln \omega) = \int\limits_{t}^{t+T} \left[\widehat{\omega}_i S_{ij} \widehat{\omega}_j - \widetilde{f}(\ln \omega) \right] dt', \tag{42}$$

24

where $\widetilde{f}(\ln\omega) = \frac{f(\omega)}{\omega}$. Due to the modeling assumption on the relaxation term, it gives a non-zero contribution only to the first coefficient,

$$B_1(\chi) = \lambda - \widetilde{f}(\chi). \tag{43}$$

For $m \geq 2$, only the vorticity stretching fluctuations from our model contribute to the Kramers-Moyal coefficients. Due to the model assumptions, we consider the $T \to 0$ limit in Eq. (40) to be effectively $\frac{T}{\tau_S} \to 0$,

$$B_m(\chi) = \lim_{T/\tau_S \to 0} \frac{1}{T} \langle \Gamma_\omega(T)^m | \ln\omega = \chi \rangle, \tag{44}$$

where Γ_ω is given by Eq. (16). The application of large-deviation statistics requires the $T \to \infty$ limit, which can be interpreted in this framework as $\frac{T}{\tau_\Omega} \to \infty$. In this limit of large integration time, where the large-deviation formalism is applicable, it is clear from Eq. (18) that the cumulant-generating function of Γ is given by

$$L_{\gamma_\omega}(q)T = \ln\langle \exp(q\Gamma_\omega) \rangle, \tag{45}$$

so that the moment-generating function is,

$$\exp(L_{\gamma_\omega}(q)T) = \langle \exp(q\Gamma_\omega) \rangle. \tag{46}$$

The moments, $\langle \Gamma_\omega(T)^m \rangle$, necessary to find the Kramers-Moyal coefficients can be computed via differentiation of the moment-generating function at the origin. For $m \geq 2$, by construction, the model gives constant coefficients. From Eq. (44), using the moment-generating function one obtains,

$$B_m(\chi) = \lim_{T/\tau_S \to 0} \frac{1}{T} \frac{d^m}{dq^m} \exp(L_{\gamma_\omega}(q)T)\bigg|_{q=0} = L_{\gamma_\omega}^{(m)}(0). \tag{47}$$

Thus, the Kramers-Moyal coefficients are given by the derivatives of the generalized Lyapunov exponent at the origin. Note that $\lambda_\omega = L'_{\gamma_\omega}(0)$ is the contribution to the $m = 1$ coefficient as shown above. The Kramers-Moyal equation for $p_{\ln\omega}(\chi, T)$ based on the model is given by

$$\frac{\partial p_{\ln\omega}}{\partial T} = -\frac{\partial}{\partial\chi}\left[(\lambda_\omega - \widetilde{f}(\chi))p_{\ln\omega}\right] + \sum_{m=2}^{\infty} \frac{(-1)^m}{m!} L_{\gamma_\omega}^{(m)}(0) \frac{\partial^m p_{\ln\omega}}{\partial\chi^m}. \tag{48}$$

The stationary distribution can be found by setting the time-derivative to zero,

$$0 = -\frac{d}{d\chi}\left[(\lambda_\omega - \widetilde{f}(\chi))p_{\ln\omega}\right] + \sum_{m=2}^{\infty} \frac{(-1)^m}{m!} L_{\gamma_\omega}^{(m)}(0) \frac{d^m p_{\ln\omega}}{d\chi^m}. \tag{49}$$

In general, this is an infinite-order ODE with variable coefficients, making analytical progress difficult. For the case of linear relaxation, the coefficients become constant, i.e. $f(\chi) = \frac{1}{\tau}$, making some analytical progress possible. Appendix A shows that the solution to the Kramers-Moyal equation gives a power-law for the tail of the stationary PDF of vorticity magnitude when linear relaxation is considered, in agreement with the stationary distribution derived by Ref. [40] for polymer lengths with linear relaxation. Nonetheless, seeing from Fig. 6 that this is not the case, another means of simplification to enable analytical progress is sought.

E. Results Using a Parabolic Cramér Function

Following Ref. [41], an approximation can be obtained by representing the Cramér function as a parabola, i.e. Gaussian statistics, Eq. (23). This amounts to truncating the Kramers-Moyal expansion at second-order, since all higher cumulants are zero for Gaussian statistics. In this case, the first two cumulants, λ_ω and Δ_ω, fully characterize the statistics and the stationary PDF must satisfy,

$$0 = -\frac{d}{d\chi}\left[(\lambda\tau_\eta - \widetilde{f}(\chi))p_{\ln\omega\tau_\eta}\right] + \frac{\Delta_\omega\tau_\eta}{2}\frac{d^2 p_{\ln\omega\tau_\eta}}{d\chi^2}. \tag{50}$$

This truncation of the Kramser-Moyal equation at second-order reduces to a Fokker-Planck equation.

The solution has the form,

$$p_{\ln\omega\tau_\eta}(\chi) = C\exp\left(\frac{2\lambda_\omega}{\Delta_\omega}\chi - \frac{2}{\Delta_\omega\tau_\eta}\int^\chi \widetilde{f}(x)dx\right), \tag{51}$$

with $\widetilde{f}(\chi) = A\exp[(n-1)\chi]$,

$$p_{\ln\omega\tau_\eta}(\chi) = C\exp\left(\frac{2\lambda_\omega}{\Delta_\omega}\chi - \frac{2A}{(n-1)\Delta_\omega\tau_\eta}\exp[(n-1)\chi]\right), \tag{52}$$

and after change of variables to vorticity magnitude,

$$p_{\omega\tau_\eta}(w) = Cw^{-1+\frac{2\lambda}{\Delta}}\exp\left(-\frac{2A}{(n-1)\Delta_\omega\tau_\eta}w^{n-1}\right), \tag{53}$$

and enstrophy,

$$p_{\omega^2\tau_\eta^2}(\xi) = C'\xi^{-1+\frac{\lambda}{\Delta}}\exp\left(-\frac{2A}{(n-1)\Delta_\omega\tau_\eta}\xi^{(n-1)/2}\right). \tag{54}$$

Therefore, the parabolic Cramér function approximation to the Kramers-Moyal model gives a stretched exponential for the stationary PDF of enstrophy in isotropic turbulence. As discussed in the development of the model, it is only designed for applicability in the tails of the PDF, therefore the interpretation of this result is that the model gives stretched-exponential tails with a power-law correction. In fact, the power-law correction with exponent $-1 + \frac{\lambda}{\Delta} \approx -0.18$ is quite small and has very little effect on the following plots.

A first test of the model PDF is to test the proposed relationship, derived from Eq. (54),

$$-\log\left(\xi^{1-\frac{\lambda}{\Delta}} p_{\omega^2 \tau_\eta^2}(\xi)\right) = \frac{2A}{(n-1)\Delta_\omega \tau_\eta} \xi^{(n-1)/2} - \log C', \tag{55}$$

by observation of a linear relationship on a plot of $-\log\left(\xi^{1-\frac{\lambda}{\Delta}} p_{\omega^2 \tau_\eta^2}(\xi)\right)$ against $\xi^{(n-1)/2}$. The result, shown in Fig. 7, indicates the success of the model, particularly in predicting the exponent $(n-1)/2 = 0.231$ (again, suggestive of $1/4$).
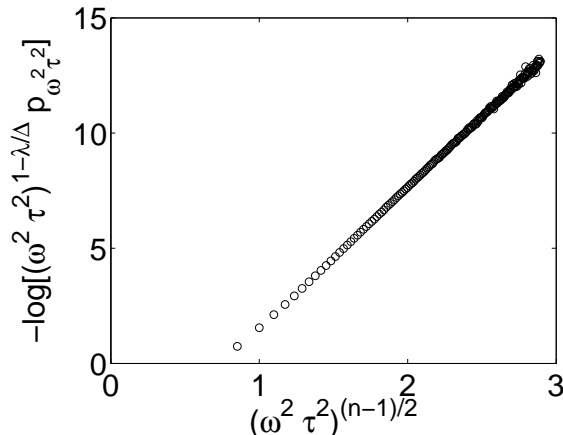

FIG. 7. Plot of $-\log\left(\xi^{1-\frac{\lambda}{\Delta}} p_{\omega^2 \tau_\eta^2}(\xi)\right)$ against $\xi^{(n-1)/2}$, for which the model successfully predicts a linear relationship. In this plot, $n = 1.462$, $\lambda = 0.100/\tau_\eta$, $\Delta = 0.122/\tau_\eta$.

The slope in Fig. 7 is the pre-factor $\frac{2A}{(n-1)\Delta_\omega \tau_\eta}$, for which there was found to be a 35% difference between the DNS PDF and the model PDF, as illustrated in Fig. 8. Figure 8a compares Eq. (54) with the observed enstrophy PDF from the isotropic DNS. The model is fully specified up to a (normalization) coefficient by the values previously determined: $A = 0.129$, $n = 1.462$, $\lambda_\omega \tau_\eta = 0.100$, and $\Delta_\omega \tau_\eta = 0.122$. The exponent $(n-1)/2 = 0.231$ is in agreement with the values found by Ref. [43]. However, from inspecting the figure, the tail of the PDF is evidently too heavy, suggesting that the coefficient $\frac{2A}{(n-1)\Delta_\omega \tau_\eta}$ is too small.

27

Indeed, increasing the viscous relaxation coefficient A by 35% leads to very good agreement with the DNS statistics, as shown in Fig. 8.
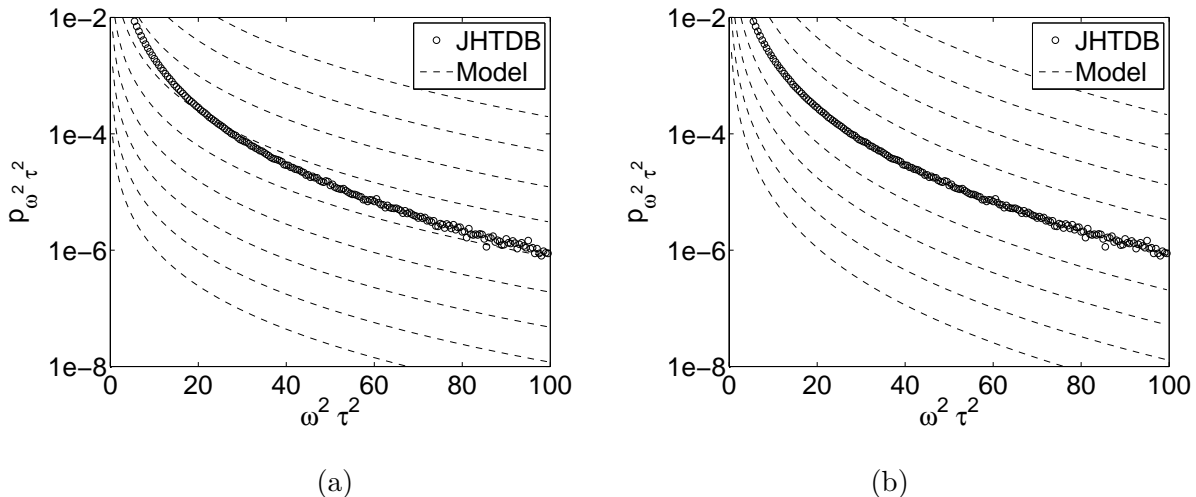

FIG. 8. Comparison of enstrophy PDF, normalized by Kolmogorov timescale τ_η, from truncated Kramers-Moyal model with JHTDB DNS-generated statistics using (a) pre-determined model parameters, $A = 0.129$, $n = 1.462$, $\lambda = 0.100/\tau_\eta$, $\Delta = 0.122/\tau_\eta$, and (b) adjusting only $A = 0.174$ to give excellent agreement with DNS enstrophy PDF.

The success outlined in Fig. 7 emphasizes the utility of the modeling approach. Before any DNS data is used, the stochastic model predicts a stretched exponential form (with small power-law correction) that has become common in fitting enstrophy PDFs. Then, once the DNS data in introduced in terms of λ and Δ from the Cramér function of cumulative vorticity stretching and n from power-law fit to the conditional mean of the viscous Laplacian, Fig. 7 shows that the model also predicts an accurate exponent, $(n-1)/2$. On the other hand, Fig. 8 provides a caveat, that the parameter A determined from the DNS needs extra adjustment for full agreement with the PDF from DNS.

Pawula's theorem [87] warns against truncation of the Kramers-Moyal equation at higher than second-order, this being similar in nature to cumulant-discard approximations. Indeed, numerical calculations (not shown) of the Kramers-Moyal model truncated after the fourth-order term resulted in negative probabilities. Therefore, while the truncation of the Kramers-Moyal expansion at second-order is less than ideal, better options are not apparent.

28

VI. CONCLUSIONS

The growth of infinitesimal material lines in isotropic turbulence is commonly described by the cumulative stretching by the strain-rate along Lagrangian trajectories, i.e. finite-time Lyapunov exponents, whose statistical behavior is governed by a large deviation principle. The evolution of vorticity along Lagrangian paths is similar to that of material lines, with important caveats, such as the two-way coupling between strain-rate and vorticity. In this paper, it is hypothesized that the cumulative vorticity stretching $\int \frac{\omega_i S_{ij} \omega_j}{\omega^2} dt$ along Lagrangian paths also has a large deviation principle governing the asymptotic evolution of its PDF. This is confirmed by noting the linear growth of the cumulant-generating function for large enough integration times. As a result, the large-deviation formalism is available to describe the statistical behavior of cumulative vorticity stretching and provides a more in-depth way to compare the statistics of vorticity stretching with material line stretching.

The Cramér function of vorticity stretching was computed from isotropic DNS at $Re_\lambda = 433$ from the Johns Hopkins Turbulence Databases (JHTDB). The Cramér function for vorticity stretching confirmed that the mean vorticity stretching is less than the mean material line stretching, as was previously known. In addition to this, other characteristics of the Cramér functions were compared, giving a comparison between cumulative vorticity stretching and FTLE statistics. The mean, variance, skewness and excess kurtosis of the cumulative vorticity stretching, γ_ω, was shown to fall in between the maximal and intermediate FTLEs, γ_1 and γ_2 respectively. Overall, the statistics of γ_ω were shown to be more similar to γ_1 than γ_2, which helps put the differences between vorticity stretching and material line stretching in perspective. In particular, the Cramér function for γ_ω showed that cumulative vorticity stretching PDFs display the same non-Gaussian tendencies as for γ_1; both of these distributions indicate more probable large positive fluctuations than negative. In the case of γ_1, this is caused at least in part by the incompressibility constraint that prevents $\gamma_1 < 1$ occurrences by definition. It is interesting to note that no such constraint exists for the vorticity stretching.

In the final section, a stochastic model using information from the vorticity stretching Cramér function was proposed for the logarithm of vorticity magnitude in high vorticity regions (i.e. in the tail of the enstrophy PDF). The model gives a stretched-exponential with small power-law correction for the tail of the enstrophy PDF. When parameters from

the Cramér function and conditional statistics measured from DNS are used, the stretched exponential matches well with exponent $n \approx 3/2$, but the pre-factor A is seen to be too low by about 35%. This is most likely indicative of the modeling error involved in assuming a separation of time-scales between strain-rate stretching and viscous relaxation effects.

ACKNOWLEDGMENTS

Appendix A: Kramers-Moyal Solution for Linear Relaxation

We briefly demonstrate a solution to the Kramers-Moyal model for the stationary PDF by considering linear relaxation, i.e., when the viscous term in Eq. (5) is linear ($n = 1$) in vorticity magnitude with a relaxation time $\tau = \frac{1}{A}$,

$$f(\omega) = -\nu \widehat{\omega}_i \frac{\partial^2 \omega_i}{\partial x_j \partial x_j} = \frac{\omega}{\tau}. \tag{A1}$$

As a result, the evolution of $\ln \omega$ becomes,

$$\frac{d \ln \omega}{dt} = \widehat{\omega}_i S_{ij} \widehat{\omega}_j - \frac{1}{\tau}, \tag{A2}$$

that is, the relaxation function is a constant, $\widetilde{f}(\ln \omega) = \frac{1}{\tau}$. This scenario was considered by Ref. [40] in the context of polymer stretching.

Under this assumption, the Kramers-Moyal model for the stationary PDF, Eq. (49), yields a constant-coefficient ordinary differential equation in χ of infinite order. The relaxation can be absorbed into the generalized Lyapunov exponents by defining,

$$\widetilde{L}(q) = L(q) - \frac{q}{\tau}, \tag{A3}$$

which is the Legendre transform of a shifted Cramér function,

$$\widetilde{S}(g) = \sup_q \left[gq - \widetilde{L}(q) \right] = \sup_q \left[\left(g + \frac{1}{\tau} \right) q - L(q) \right] = S\left(g + \frac{1}{\tau} \right). \tag{A4}$$

With this modified generalized Lyapunov exponent, the equation for the stationary distribution becomes,

$$0 = \sum_{m=1}^{\infty} \frac{(-1)^m}{m!} \widetilde{L}^{(m)}(0) \frac{d^m p_{\ln \omega}}{d\chi^m}. \tag{A5}$$

30

We can solve this differential equation on a semi-infinite domain (i.e. for the right-hand side 'tail' region of the PDF) using a Laplace transform. Utilizing the properties of derivatives under Laplace transformation, the equation for the stationary distribution in Laplace space becomes,

$$C(s) = \widehat{p}_{\ln \omega}(s) \sum_{m=1}^{\infty} \frac{(-s)^m}{m!} \widetilde{L}^{(m)}(0), \tag{A6}$$

where $C(s)$ is an analytic function arising from the necessity to specify boundary conditions in probability space. In this form, the summation is seen to be a Taylor expansion of the generalized Lyapunov exponent about zero, so

$$C(s) = \widehat{p}_{\ln \omega}(s) \widetilde{L}(-s). \tag{A7}$$

The stationary distribution can be constructed by solving for $\widehat{p}_{\ln \omega}(s)$ and performing the inverse Laplace transform via contour integration in the complex plane. Because $C(s)$ is an analytic function, the only poles contributing to this inverse transform come from the zeros of $\widetilde{L}(-s)$.

Constraints on the generalized Lyapunov exponent, namely that $\widetilde{L}(0) = 0$ and $L''(q) \geq 0$, require that there be at most two first-order zeros with one being at $q = 0$ and the other being at $q = q^*$ (or one second-order zero at $q = 0$). The form of the stationary distribution is thus,

$$p_{\ln \omega}(\chi) = A_1 + A_2 \exp(-q^* \chi). \tag{A8}$$

The decay of the PDF to zero at infinity requires $A_1 = 0$. By changing variables from $\ln \omega$ to ω, the PDF for the vorticity magnitude becomes a power-law,

$$p_\omega(w) = A_2 w^{-1-q^*}, \tag{A9}$$

in agreement with the results of Ref. [40].

As a caveat, the conditional statistics in Fig. 6 clearly show that the viscous destruction of vorticity increases super-linearly ($n > 1$) with increasing vorticity magnitude, and therefore a linear model is ill-equipped to describe the vorticity statistics. Nonetheless, this appendix shows that the Kramers-Moyal model constructed here produces a known result for the case

31

of linear relaxation.

---

[1] A. N. Kolmogorov, "The local structure of turbulence in incompressible viscous fluid for very large Reynolds numbers," *Dokl. Akad. Nauk SSSR*, vol. 30, pp. 299–303, 1941.

[2] H. Tennekes and J. L. Lumley, *A First Course in Turbulence.* Cambridge, MA: MIT Press, 1972.

[3] S. B. Pope, *Turbulent Flows.* Cambridge, UK: Cambridge University Press, 2000.

[4] C. Meneveau, "Lagrangian Dynamics and Models of the Velocity Gradient Tensor in Turbulent Flows," *Annual Review of Fluid Mechanics*, vol. 43, pp. 219–245, Jan. 2011.

[5] J. M. Wallace, "Twenty years of experimental and direct numerical simulation access to the velocity gradient tensor: What have we learned about turbulence?," *Physics of Fluids*, vol. 21, no. 2, p. 021301, 2009.

[6] K. R. Sreenivasan and R. A. Antonia, "The Phenomenology of Small-Scale Turbulence," *Annual Review of Fluid Mechanics*, vol. 29, pp. 435–472, Jan. 1997.

[7] A. N. Kolmogorov, "A refinement of previous hypotheses concerning the local structure of turbulence in a viscous incompressible fluid at high Reynolds number," *Journal of Fluid Mechanics*, vol. 13, pp. 82–85, Mar. 1962.

[8] A. M. Oboukhov, "Some specific features of atmospheric tubulence," *Journal of Fluid Mechanics*, vol. 13, pp. 77–81, Mar. 1962.

[9] G. Parisi and U. Frisch, "On the singularity structure of fully developed turbulence," in *Turbulence and Predictability in Geophysical Fluid Dynamics* (M. Ghil, R. Benzi, and G. Parisi, eds.), North-Holland, New York, 1985.

[10] U. Frisch, *Turbulence: The Legacy of A. N. Kolmogorov.* Cambridge University Press, 1995.

[11] C. Meneveau and K. R. Sreenivasan, "The multifractal nature of turbulent energy dissipation," *Journal of Fluid Mechanics*, vol. 224, pp. 429–484, Apr. 1991.

[12] R. M. Kerr, "Higher-order derivative correlations and the alignment of small-scale structures in isotropic numerical turbulence," *Journal of Fluid Mechanics*, vol. 153, pp. 31–58, Apr. 1985.

[13] R. Kerr, "Histograms of helicity and strain in numerical turbulence," *Physical Review Letters*, vol. 59, pp. 783–786, Aug. 1987.

[14] W. T. Ashurst, A. R. Kerstein, R. M. Kerr, and C. H. Gibson, "Alignment of vorticity and

scalar gradient with strain rate in simulated NavierStokes turbulence," *Physics of Fluids*, vol. 30, no. 8, pp. 2343–2353, 1987.

[15] S. Kida and K. Ohkitani, "Spatiotemporal intermittency and instability of a forced turbulence," *Physics of Fluids A: Fluid Dynamics*, vol. 4, no. 5, p. 1018, 1992.

[16] K. Ohkitani and S. Kishiba, "Nonlocal nature of vortex stretching in an inviscid fluid," *Physics of Fluids*, vol. 7, no. 2, p. 411, 1995.

[17] K. K. Nomura and G. K. Post, "The structure and dynamics of vorticity and rate of strain in incompressible homogeneous turbulence," *Journal of Fluid Mechanics*, vol. 377, pp. 65–97, 1998.

[18] D. I. Pullin and P. G. Saffman, "Vortex Dynamics in Turbulence," *Annual Review of Fluid Mechanics*, vol. 30, pp. 31–51, Jan. 1998.

[19] M. Guala, B. Luthi, A. Liberzon, A. Tsinober, and W. Kinzelbach, "On the evolution of material lines and vorticity in homogeneous turbulence," *Journal of Fluid Mechanics*, vol. 533, pp. 339–359, June 2005.

[20] B. Luthi, A. Tsinober, and W. Kinzelbach, "Lagrangian measurement of vorticity dynamics in turbulent flow," *Journal of Fluid Mechanics*, vol. 528, pp. 87–118, Apr. 2005.

[21] T. Ishihara, T. Gotoh, and Y. Kaneda, "Study of High Reynolds Number Isotropic Turbulence by Direct Numerical Simulation," *Annual Review of Fluid Mechanics*, vol. 41, pp. 165–180, Jan. 2009.

[22] M. Holzner, M. Guala, B. Luthi, A. Liberzon, N. Nikitin, W. Kinzelbach, and A. Tsinober, "Viscous tilting and production of vorticity in homogeneous turbulence," *Physics of Fluids*, vol. 22, no. 6, p. 061701, 2010.

[23] A. Vincent and M. Meneguzzi, "The spatial structure and statistical properties of homogeneous turbulence," *Journal of Fluid Mechanics*, vol. 225, pp. 1–20, Apr. 1991.

[24] Z.-S. She, E. Jackson, and S. A. Orszag, "Sturcture and dynamics of homogeneous turbulence: models and simulations," *Proceedings of the Royal Society of London A*, vol. 434, pp. 101–124, 1991.

[25] J. Jiménez, A. A. Wray, P. G. Saffman, and R. S. Rogallo, "The structure of intense vorticity in isotropic turbulence," *Journal of Fluid Mechanics*, vol. 255, pp. 65–90, Apr. 1993.

[26] J. Jiménez and A. A. Wray, "On the characteristics of vortex filaments in isotropic turbulence," *Journal of Fluid Mechanics*, vol. 373, pp. 255–285, Oct. 1998.

[27] A. Y.-S. Kuo and S. Corrsin, "Experiment on the geometry of the fine-structure regions in fully turbulent fluid," *Journal of Fluid Mechanics*, vol. 56, pp. 447–479, Mar. 1972.

[28] K. Bürger, M. Treib, R. Westermann, S. Werner, C. C. Lalescu, A. Szalay, C. Meneveau, and G. L. Eyink, "Vortices within vortices: hierarchical nature of vortex tubes in turbulence," *arXiv*, Oct. 2013.

[29] A. A. Townsend, "On the Fine-Scale Structure of Turbulence," *Proceedings of the Royal Society of London A*, vol. 208, no. 1095, pp. 534–542, 1951.

[30] H. Tennekes, "Simple model for the small-scale structure of turbulence," *Phys. Fluids*, vol. 11, pp. 669–671, 1968.

[31] T. S. Lundgren, "Strained spiral vortex model for turbulent fine structure," *Physics of Fluids*, vol. 25, no. 12, pp. 2193–2203, 1982.

[32] A. J. Chorin, "Turbulence and vortex stretching on a lattice," *Communications on Pure and Applied Mathematics*, vol. 39, no. S1, pp. S47–S65, 1986.

[33] A. J. Chorin, "Scaling laws in the vortex lattice model of turbulence," *Communications in Mathematical Physics*, vol. 114, pp. 167–176, Mar. 1988.

[34] D. I. Pullin and P. G. Saffman, "On the LundgrenTownsend model of turbulent fine scales," *Physics of Fluids A: Fluid Dynamics*, vol. 5, pp. 126–145, Jan. 1993.

[35] P. L. Johnson and C. Meneveau, "Large-deviation joint statistics of the finite-time Lyapunov spectrum in isotropic turbulence," *Physics of Fluids*, vol. 27, no. 8, p. 085110, 2015.

[36] L. Biferale, C. Meneveau, and R. Verzicco, "Deformation statistics of sub-Kolmogorov-scale ellipsoidal neutrally buoyant drops in isotropic turbulence," *Journal of Fluid Mechanics*, vol. 754, pp. 184–207, July 2014.

[37] G. I. Taylor, "Production and Dissipation of Vorticity in a Turbulent Fluid," *Proceedings of the Royal Society of London. Series A, Mathematical and Physical Sciences*, vol. 164, no. 916, pp. 15–23, 1938.

[38] A. Tsinober, *An Informal Conceptual Introduction to Turbulence.* Springer, 2nd ed., 2009.

[39] M.-J. Huang, "Correlations of vorticity and material line elements with strain in decaying turbulence," *Physics of Fluids*, vol. 8, no. 8, p. 2203, 1996.

[40] E. Balkovsky, A. Fouxon, and V. Lebedev, "Turbulent Dynamics of Polymer Solutions," *Physical Review Letters*, vol. 84, pp. 4765–4768, May 2000.

[41] M. Chertkov, "Polymer Stretching by Turbulence," *Physical Review Letters*, vol. 84, no. 20,

pp. 4761–4764, 2000.

[42] A. Bershadskii, E. Kit, and A. Tsinober, "On universality of geometrical invariants in turbulenceExperimental results," *Physics of Fluids A: Fluid Dynamics*, vol. 5, no. 1993, p. 1523, 1993.

[43] D. A. Donzis, P. K. Yeung, and K. R. Sreenivasan, "Dissipation and enstrophy in isotropic turbulence: Resolution effects and scaling in direct numerical simulations," *Physics of Fluids*, vol. 20, no. 4, p. 045108, 2008.

[44] S. S. Girimaji and S. B. Pope, "Material-element deformation in isotropic turbulence," *Journal of Fluid Mechanics*, vol. 220, pp. 427–458, Apr. 1990.

[45] H. Xu, A. Pumir, and E. Bodenschatz, "The pirouette effect in turbulent flows," *Nature Physics*, vol. 7, pp. 709–712, June 2011.

[46] L. Chevillard and C. Meneveau, "Lagrangian time correlations of vorticity alignments in isotropic turbulence: Observations and model predictions," *Physics of Fluids*, vol. 23, no. 10, p. 101704, 2011.

[47] J. Boschung, P. Schaefer, N. Peters, and C. Meneveau, "The local topology of stream- and vortex lines in turbulent flows," *Physics of Fluids*, vol. 26, p. 045107, Apr. 2014.

[48] H. Cramer, "Sur un nouveau theoreme-limite de la theorie des probabilites," *Actualites Scientifiques et Industrielles*, vol. 736, pp. 5–23, 1938.

[49] J. Gartner, "On large deviations from the invariant measure," *Theory of Probability and Its Applications*, vol. 22, pp. 24–39, 1977.

[50] R. S. Ellis, "Large deviations for a general class of random vectors," *The Annals of Probability*, vol. 12, no. 1, pp. 1–12, 1984.

[51] M. Donsker and S. R. S. Varadhan, "Asymptotic Evaluation of Certain Markov Process Expectations for Large Time, I," *Communications on Pure and Applied Mathematics*, vol. XXVIII, pp. 1–47, 1975.

[52] M. Donsker and S. R. S. Varadhan, "Asymptotic Evaluation of Certain Markov Process Expectations for Large Time, II," *Communications on Pure and Applied Mathematics*, vol. XXVIII, pp. 279–301, 1975.

[53] M. Donsker and S. R. S. Varadhan, "Asymptotic evaluation of certain Markov process expectations for large time, III," *Communications on Pure and Applied Mathematics*, vol. XXIX, pp. 389–461, 1976.

[54] M. D. Donsker and S. R. S. Varadhan, "Asymptotic evaluation of certain markov process expectations for large time, IV," *Communications On Pure And Applied Mathematics*, vol. 36, pp. 183–212, 1983.

[55] B. B. Mandelbrot, "Intermittent turbulence i n self-similar cascades : divergence of high moments and dimension of the carrier," *Journal of Fluid Mechanics*, vol. 62, no. 2, pp. 331–358, 1974.

[56] C. Evertsz and B. Mandelbrot, "Multifractal measures," in *Chaos and Fractals* (H.-O. Peitgen, H. Jurgens, and D. Saupe, eds.), pp. 921–953, Berlin: Springer, 1992.

[57] T. Watanabe, Y. Nakayama, and H. Fujisaka, "Large deviation statistics of the energy-flux fluctuation in the shell model of turbulence," *Physical review. E, Statistical physics, plasmas, fluids, and related interdisciplinary topics*, vol. 61, no. 2, pp. R1024–1027, 2000.

[58] Y. Nakayama, T. Watanabe, and H. Fujisaka, "Self-similar fluctuation and large deviation statistics in the shell model of turbulence," *Physical Review E*, vol. 64, p. 056304, 2001.

[59] E. Balkovsky and A. Fouxon, "Universal long-time properties of Lagrangian statistics in the Batchelor regime and their application to the passive scalar problem.," *Physical review. E, Statistical physics, plasmas, fluids, and related interdisciplinary topics*, vol. 60, no. 4, pp. 4164–4174, 1999.

[60] F. Bagheri, D. Mitra, P. Perlekar, and L. Brandt, "Statistics of polymer extensions in turbulent channel flow," *Physical Review E*, vol. 86, p. 056314, Nov. 2012.

[61] M. Vucelja, K. S. Turitsyn, and M. Chertkov, "Extreme value statistics of work done in stretching a polymer in a gradient flow," *Physical Review E*, vol. 91, p. 022123, 2015.

[62] E. Balkovsky, G. Falkovich, and A. Fouxon, "Intermittent distribution of inertial particles in turbulent flows," *Physical Review Letters*, vol. 86, no. 13, pp. 2790–2793, 2001.

[63] J. Bec, L. Biferale, G. Boffetta, M. Cencini, S. Musacchio, and F. Toschi, "Lyapunov exponents of heavy particles in turbulence," *Physics of Fluids*, vol. 18, p. 091702, 2006.

[64] G. Falkovich, K. Gawedski, and M. Vergassola, "Particles and fields in fluid turbulence," *Rev. Mod. Phys.*, vol. 73, no. October, pp. 913–975, 2001.

[65] J. Miller, "Statistical mechanics of Euler equations in two dimensions," *Physical review letters*, vol. 65, no. 17, pp. 2137–2140, 1990.

[66] R. Robert, "A maximum-entropy principle for two-dimensional perfect fluid dynamics," *Journal of Statistical Physics*, vol. 65, pp. 531–553, 1991.

[67] R. Robert and J. Sommeria, "Relaxation Towards a Statistical Equilibrium State in Two-Dimensional Perfect Fluid Dynamics," *Physical Review Letters*, vol. 69, no. 19, pp. 2776–2779, 1992.

[68] F. Bouchet and A. Venaille, "Statistical mechanics of two-dimensional and geophysical flows," *Physics Reports*, vol. 515, no. 5, pp. 227–295, 2012.

[69] G. Boffetta, A. Celani, S. Musacchio, and M. Vergassola, "Intermittency in two-dimensional Ekman-Navier-Stokes turbulence," *Physical Review E*, vol. 66, p. 026304, 2002.

[70] F. Bouchet and E. Simonnet, "Random Changes of Flow Topology in Two-Dimensional and Geophysical Turbulence," *Physical Review Letters*, vol. 102, p. 094504, 2009.

[71] F. Bouchet, J. Laurie, and O. Zaboronski, "Langevin Dynamics, Large Deviations and Instantons for the Quasi-Geostrophic Model and Two-Dimensional Euler Equations," *Journal of Statistical Physics*, vol. 156, pp. 1066–1092, 2014.

[72] H. Yu and C. Meneveau, "Lagrangian Refined Kolmogorov Similarity Hypothesis for Gradient Time Evolution and Correlation in Turbulent Flows," *Physical Review Letters*, vol. 104, p. 084502, Feb. 2010.

[73] H. Yu and C. Meneveau, "Scaling of Conditional Lagrangian Time Correlation Functions of Velocity and Pressure Gradient Magnitudes in Isotropic Turbulence," *Flow, Turbulence and Combustion*, vol. 85, pp. 457–472, Apr. 2010.

[74] R. Benzi, G. Paladin, G. Parisi, and A. Vulpiani, "Characterisation of intermittency in chaotic systems," *Journal of Physics A*, vol. 18, pp. 2157–2165, Aug. 1985.

[75] J.-P. Eckmann and I. Procaccia, "Fluctuations of Dynamical Scaling Indices in Nonlinear Systems," *Physical Review A*, vol. 34, no. 1, pp. 659–661, 1986.

[76] G. Paladin and A. Vulpiani, "Anomalous scaling laws in multifractal objects," *Physics Reports*, vol. 156, pp. 147–225, Dec. 1987.

[77] Y. Li, E. Perlman, M. Wan, Y. Yang, C. Meneveau, R. Burns, S. Chen, A. Szalay, and G. Eyink, "A public turbulence database cluster and applications to study Lagrangian evolution of velocity increments in turbulence," no. August 2015, p. 30, 2008.

[78] E. Perlman, R. Burns, Y. Li, and C. Meneveau, "Data exploration of turbulence simulations using a database cluster," *Proceedings of the 2007 ACM/IEEE Conference on Supercomputing (SC '07)*, 2007.

[79] H. Yu, K. Kanov, E. Perlman, J. Graham, E. Frederix, R. Burns, A. Szalay, G. Eyink, and

C. Meneveau, "Studying Lagrangian dynamics of turbulence using on-demand fluid particle tracking in a public turbulence database," *Journal of Turbulence*, vol. 13, no. August 2015, p. N12, 2012.

[80] E. Dresselhaus and M. Tabor, "The kinematics of stretching and alignment of material elements in general flow fields," *Journal of Fluid Mechanics*, vol. 236, pp. 415–444, Apr. 1991.

[81] M. Wilczek and R. Friedrich, "Dynamical origins for non-Gaussian vorticity distributions in turbulent flows," *Physical Review E*, vol. 80, p. 016316, 2009.

[82] T. S. Lundgren, "Distribution Functions in the Statistical Theory of Turbulence," *Physics of Fluids*, vol. 10, no. 5, pp. 969–975, 1967.

[83] A. Monin, "Equations of turbulent motion," *Prikl. Mat. Mekh.*, vol. 31, no. 6, pp. 1057–1068, 1967.

[84] E. A. Novikov, "Kinetic equations for a vortex field," *Soviet Physics Doklady*, vol. 12, p. 1006, 1968.

[85] C. M. White and M. G. Mungal, "Mechanics and Prediction of Turbulent Drag Reduction with Polymer Additives," *Annual Review of Fluid Mechanics*, vol. 40, pp. 235–256, Jan. 2008.

[86] R. H. Kraichnan, "Small-Scale Structure of a Scalar Field Convected by Turbulence," *Physics of Fluids*, vol. 11, no. 5, p. 945, 1968.

[87] R. F. Pawula, "Approximation of the Linear Boltzmann Equation by the Fokker-Planck Equation," *Physical Review*, vol. 162, no. 1, pp. 186–188, 1967.